JOURNAL OF AIRCRAFT
Vol. 33, No. 4, July–August 1996

Flow About a Slotted Cylinder–Airfoil Combination in a Wind Tunnel

Paul G. A. Cizmaş,* Deman Tang,† and Earl H. Dowell‡
Duke University, Durham, North Carolina 27708-0300

The flowfield around a gust generator device, an airfoil/rotating slotted cylinder (RSC) system, is numerically simulated using the general-purpose finite element program FIDAP. The flow is assumed to be quasisteady, turbulent, incompressible, and two dimensional. The turbulence is modeled far from the walls by a high Reynolds number k-ε model. In the near-wall region, which includes the viscous sublayer, the mixing length concept is used to model turbulence. The numerical analysis treats the time-varying flow around the gust generator device as quasisteady and solves the flow position-by-position as the RSC rotates. The variation of lift and drag as a function of the rotation angle and as a function of the gap between the airfoil and the rotating slotted cylinder is calculated.

Nomenclature

C_D = drag coefficient, $0.5\rho V^2 d$
C_L = lift coefficient, $0.5\rho V^2 d$
$C_{L\text{eq}}$ = equivalent lift coefficient, $0.5\rho V^2(c + d)$
C_μ, C_1, C_2 = constants of the k-ε turbulence model
c = airfoil chord
d = exterior diameter of RSC
e = gap between the o.d. of RSC and the trailing edge of the airfoil
f_i = external force in x_i direction
h = height of wind-tunnel test section
I = wind-tunnel turbulence number
k = turbulent kinetic energy
l = length of wind-tunnel test section
p = pressure
R_μ = constant
t = time
t_C = RSC thickness
u_i = mean velocity component in x_i direction
u, v = mean velocity components in x and y direction
V = inlet velocity in the wind-tunnel test section
γ = acceleration factor
ε = viscous dissipation rate of k
θ = rotation angle
λ = penalty parameter
μ = molecular viscosity
μ_l = laminar viscosity
μ_t = eddy (or turbulent) viscosity
ρ = fluid density
σ_ε, σ_k = constants of the k-ε turbulence model

Superscript
$\bar{}$ = normalized by airfoil chord

Received Aug. 30, 1995; revision received March 21, 1996; accepted for publication March 26, 1996.

*Research Assistant, Department of Mechanical Engineering and Materials Science; currently Senior Engineer and Scientist, Westinghouse Electric Corporation, Science and Technology Center, Pittsburgh, PA 15235-5098. Member AIAA.

†Research Associate, Department of Mechanical Engineering and Materials Science.

‡J. A. Jones Professor and Dean of the School of Engineering. Fellow AIAA.

Introduction

TO study the response of structures to gust excitation, various mechanisms have been developed for creating an oscillating flow in a wind tunnel. Previous designs of gust generators have included cascades of oscillating airfoils, fixed airfoils with oscillating flaps, fixed airfoils with oscillating jet flaps, oscillating biplane vanes mounted on the side walls of the wind-tunnel test section, and airfoils with circulation control. These methods have a certain mechanical complexity to achieve the required sinusoidal lateral and longitudinal gust amplitude over the desired frequency range. The excitation system studied here is based on a fixed airfoil with a rotating slotted cylinder (RSC) at its trailing edge,[1] which combines mechanical simplicity, controllability, and reliability. This excitation system can produce high-frequency, high-force aerodynamic excitation with minimal power and torque input.

An airfoil/RSC system was built and tested in a low-speed, closed-circuit wind tunnel.[2] Two such configurations were constructed to generate a gust field and used to study the effects of changes in distance between adjacent cylinders. A simplified theoretical aerodynamic model was proposed to guide the experimental design. The flowfield was assumed to be quasisteady and the RSC was replaced by two rotating airfoils, modeled by a linear segment vortex. Comparison with the experimental results showed that the theoretical model, although useful for experimental design purposes, needed improvement for more accurate quantitative prediction.

The present report is intended to be a step toward better computational modeling of the airfoil/RSC system. To properly calculate the separated flow around the RSC, the Navier–Stokes equations with a k-ε turbulence model are used to model the flow. The main simplifying assumption made for solving the flow is that the angular velocity of the slotted cylinder is small and, as a result, the flow is quasisteady. The next two sections present the equations of the flow model and a description of the solution strategy. The results section examines the effect of the gap between the airfoil and the RSC on the lift and drag of the slotted cylinder–airfoil combination as well as the variation of lift and drag as a function of the rotation angle. The results section also presents a grid refinement study and a comparison of the numerical results with experimental data.

Model

In the wind tunnel, the flow around the airfoil/RSC is unsteady, turbulent, and three dimensional. The unsteadiness is

the result of the rapid rotation of the RSC around its axis. If one assumes that the RSC angular velocity is small enough, then the flow may be considered quasisteady, which dramatically simplifies the flow computation. A further simplification is to reduce the three-dimensional flow to a two-dimensional flow, because the span of the airfoil/RSC is much larger than the maximum dimension of its cross section (usually the length of the RSC is 6–8 times larger than its diameter). The end effects do not modify the flow pattern far away from the airfoil/RSC extremities, and so the flow can be modeled as two dimensional. Finally, because the flow speed in the wind-tunnel experiments is 20 m/s, the flow can be considered incompressible for correlation with these test data.

Given these simplifying assumptions, the flow to be computed is steady, two dimensional, incompressible, and turbulent. Because the RSC is not axisymmetric, the flow pattern depends on the RSC orientation. Because of the cross-sectional shape of the RSC, the flow pattern repeats after a rotation of 180 deg. Additional observations about the symmetry of the flow configuration and ways to reduce and check the computation are presented in the section discussing the results.

The equations governing the flow around the airfoil/RSC are the continuity equation:

$$u_{i,i} = 0 \tag{1}$$

and the Navier–Stokes equation of motion:

$$\rho u_j u_{i,j} = \rho f_i - p_{,i} + [\mu(u_{i,j} + u_{j,i})]_{,j} \tag{2}$$

The viscosity μ is modeled using Boussinesq's eddy viscosity assumption:

$$\mu = \mu_l + \mu_t$$

The turbulent viscosity μ_t is computed using k and ε:

$$\mu_t = C_\mu \rho(k^2/\varepsilon) \tag{3}$$

The equations for the kinetic energy and for the kinetic energy dissipation rate are

$$\frac{Dk}{Dt} = \frac{1}{\rho}\frac{\partial}{\partial x_k}\left(\frac{\mu_t}{\sigma_k}\frac{\partial k}{\partial x_k}\right) + \frac{\mu_t}{\rho}\left(\frac{\partial u_i}{\partial x_k} + \frac{\partial u_k}{\partial x_i}\right)\frac{\partial u_i}{\partial x_k} - \varepsilon \tag{4}$$

$$\frac{D\varepsilon}{Dt} = \frac{1}{\rho}\frac{\partial}{\partial x_k}\left(\frac{\mu_t}{\sigma_\varepsilon}\frac{\partial \varepsilon}{\partial x_k}\right) + \frac{C_1\mu_t}{\rho}\frac{\varepsilon}{k}\left(\frac{\partial u_i}{\partial x_k} + \frac{\partial u_k}{\partial x_i}\right)\frac{\partial u_i}{\partial x_k} - C_2\frac{\varepsilon^2}{k} \tag{5}$$

The constants in the equations have the values corresponding to the standard k-ε model[3]:

$$\begin{aligned} C_\mu &= 0.09 \\ C_1 &= 1.44 \\ C_2 &= 1.92 \\ \sigma_k &= 1.0 \\ \sigma_\varepsilon &= 1.3 \end{aligned} \tag{6}$$

This k-ε model is of the high Reynolds number type and is not suitable to model regions adjacent to solid boundaries that contain the viscous sublayer. In the regions adjacent to solid boundaries (the so-called near-wall regions) the Reynolds number is much lower than in the main flow and the k-ε model presented previously does not predict the turbulent viscosity well. Instead it is possible to use a low Reynolds number variant of the k-ε turbulence model. Although the turbulent viscosity can be accurately predicted using a low Reynolds number k-ε model, the rapid variation of the flow variables requires a very large number of grid points in the near-wall regions. The fine mesh size increases the computational time by an order of magnitude[4] and makes the low Reynolds number k-ε turbulence model an expensive option.

Thus, the near-wall regions are computed in this article by using specialized shape functions based on universal near-wall profiles.[5] These shape functions are used in a one-element-thick layer of special elements that includes the viscous sublayer and connects the fully turbulent outer flowfield and the physical boundary. The shape functions vary with the characteristic Reynolds number such that they can adjust to better represent the variation of the flow quantities. The k and ε equations are not solved in the layer of special near-wall elements because, as mentioned earlier, the high Reynolds model used in the fully turbulent flow is not appropriate in the viscous sublayer. Instead, the mixing length concept is used to model turbulent diffusivities of mass and momentum. By coupling the k-ε turbulence model used in the fully turbulent outer region, with the mixing length approach used for the viscous sublayer, an accurate, universal, and efficient method is obtained.

Method

Equations (1–5) completely describe the two-dimensional turbulent steady flow around the airfoil/RSC. To determine the flow variables, the general-purpose finite element program FIDAP is used. FIDAP is an integrated set of components and program modules designed to perform all aspects of the model generation, problem setup, postprocessing, and solution phases of a flow analysis. In this analysis the fluid domain is discretized using bilinear four-node quadrilateral elements. The nodal basis functions and the velocity basis functions are linear, while the pressure basis function is constant (and equal to 1). For the present assumptions, as can be seen from Eqs. (1–5), there are five unknowns per node: u, v, p, k, and ε. To reduce computational effort, the penalty function approach is used to eliminate pressure from the list of unknowns. In the first step the continuity requirement is weakened and replaced by[6]

$$u_{i,i} = -\lambda p \tag{7}$$

Recommended values for λ are in the range 10^{-5}–10^{-9}. Equation (7) is then used to eliminate pressure from the momentum Eq. (2). The pressure is computed after the solution of u, v, k, and ε is obtained, by using Eq. (7) written as

$$p = -(1/\lambda)u_{i,i}$$

Note that by using Eq. (7) instead of Eq. (1) the fluid becomes very slightly compressible.

The nonlinear system of equations that contains the u, v, k, and ε unknowns is solved by using the Picard iteration scheme (known also as successive substitution):

$$[M(u_i)]\{u_{i+1}\} = \{RHS\}$$

The nonlinearity is evaluated at the known iterate u_i and the linear system must be formed and solved at each iteration.[5] The method converges for a fair range of Reynolds numbers and is relatively insensitive to the initial guess. The drawback of the method is its slow convergence. The rate of convergence can often be improved by using γ, such that

$$[M(u_i)]\{u^*\} = \{RHS\}$$

$$u_{i+1} = u^*\gamma + (1 - \gamma)u_i$$

Because there is no theoretical basis to choose a suitable value for γ, numerical tests must be done to obtain a satisfactory value. For the airfoil/RSC the tests showed that an appropriate

choice for the acceleration factor is 0.7 for u and v and 0.3 for k and ε.

The iterative process stops when two conditions are satisfied. First, the norm of the relative error of the solution should be smaller than an imposed limit, $err1$. Second, the norm of the relative residual vector has to be smaller than a given value, $err2$. To compute the flow on the airfoil with the imposed precision $err1 = 0.01$ and $err2 = 0.001$, usually about 30 iterations are necessary. For $err1 = 0.001$ and $err2 = 0.001$ the number of iterations increases to about 60, and sometimes it is necessary to introduce artificial viscosity to suppress the numerical oscillations of k and ε. Although the artificial viscosity makes the numerical scheme more stable, increasing the viscosity may produce inaccurate results by making the scheme overly diffusive.

Results

The numerical simulation is used in this article to analyze the lift and drag variation as a function of the rotation angle and gap between the airfoil and the RSC. Three main configurations were studied. With the first configuration the influence of the gap between the airfoil and the RSC (for a fixed rotation angle) on the airfoil/RSC lift and drag was examined. The second configuration allowed the analysis of the variation of lift and drag on the RSC as a function of the rotation angle. In the second configuration the airfoil is not included in the geometry and the focus is only on the isolated RSC. In the third configuration, the airfoil/RSC lift and drag variation with the rotation angle was examined, for a fixed value of the gap between the airfoil and the RSC.

Effect of Gap Distance

The first configuration is shown in Fig. 1. The wind-tunnel test section, which represents the exterior boundary of the domain, is 1.7 m ($\bar{l} = 16.67$) long and 488 mm ($\bar{h} = 4.78$) high. The exterior diameter of the RSC is 25.4 mm ($\bar{d} = 0.25$) and the RSC thickness is 2.5 mm ($\bar{t}_C = 0.0245$). The center of the RSC is situated at 547 mm (5.36c) from the inlet in the wind-tunnel test section and is equally spaced from the wind-tunnel walls. The airfoil is a NACA 0012 profile with a chord c = 102 mm. The leading edge is 419 mm (4.11c) away from the inlet section. The angle θ, measured as shown in Fig. 1, is 70 deg. The RSC position, measured with respect to the inlet section, varies from 535.5 mm (5.25c) to 560 mm (5.49c). As a result, the gap e between the trailing edge and the RSC varies between 1.8–26.3 mm, or expressed with respect to the airfoil chord, is between 1.8–26.0% of the airfoil chord.

The flowfield boundary conditions are $u = 20$ m/s and $v = 0$ at the inlet, and $u = 0$ and $v = 0$ at the wind-tunnel walls and on the airfoil/RSC surface. No explicit boundary conditions are imposed at the outlet, where the code automatically generates a zero flux for the node unknowns. To compute the turbulent flow, boundary conditions are imposed for k and ε. At the inlet the turbulence kinetic energy is estimated using the relation:

$$k = 1.5(Iu)^2$$

For the inlet velocity $u = 20$ m/s and $I = 0.004$ one obtains $k = 0.0096$ m^2/s^2. The dissipation rate of turbulent kinetic energy at the inlet is estimated using the relation:

$$\varepsilon = \rho C_\mu (k^2/R_\mu \mu)$$

where R_μ is a constant varying for most typical flows between $\mathcal{O}(10)$ and $\mathcal{O}(100)$. The constant used to compute the turbulent viscosity [Eq. (6)] is C_μ. With the density $\rho = 1.23$ kg/m^3, laminar viscosity $\mu_l = 18 \times 10^{-6}$ Pa s, and $R_\mu = 100$, one obtains $\varepsilon = 0.0057$. Boundary conditions are not imposed for k and ε along the wind-tunnel walls and along the airfoil/RSC because the mixing length approach is used here instead of the k-ε model. The values of the initial conditions for u and v are zero everywhere in the interior of the domain. The initial conditions for k and ε in the interior of the domain have the same values as the boundary conditions for k and ε at the inlet section.

Several grid discretizations were tested. The small dimensions of the RSC as compared to the exterior boundary requires a grid with elements whose dimensions vary rapidly such that the total number of elements is reduced as much as possible. This requirement can be satisfied better by a paved grid than by a mapped grid.[7] However, the paved grid offers less control over grid generation, especially far from the boundary. The result of the tests showed that for the present configuration it is better to use a combination of paving and mapping, as presented in Fig. 2. Paved meshes with several boundary-edge layers were used around the airfoil and the RSC. The rest of the domain was discretized using mapped grids that permitted good control of elements in the RSC wake zone.

The speed contour plot represented in Fig. 3 shows the flow pattern in the vicinity of the slotted cylinder–airfoil combination for the gap $\bar{e} = 0.08$. A large separation zone exists on the interior side of the upper half of the RSC as well as on the upper right side of the lower half of the RSC. The flow is

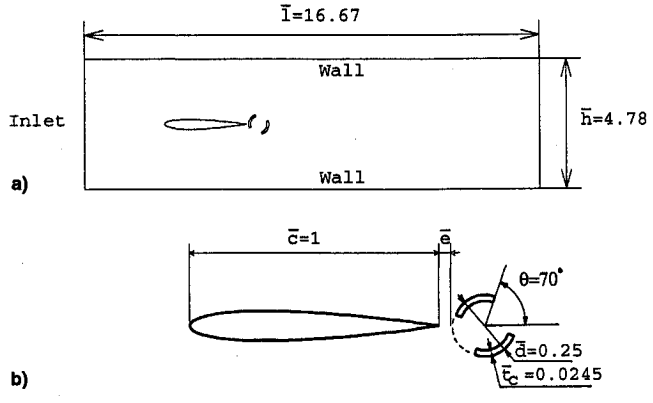

Fig. 1 Geometry of the first configuration: a) entire domain and b) detail of airfoil and RSC.

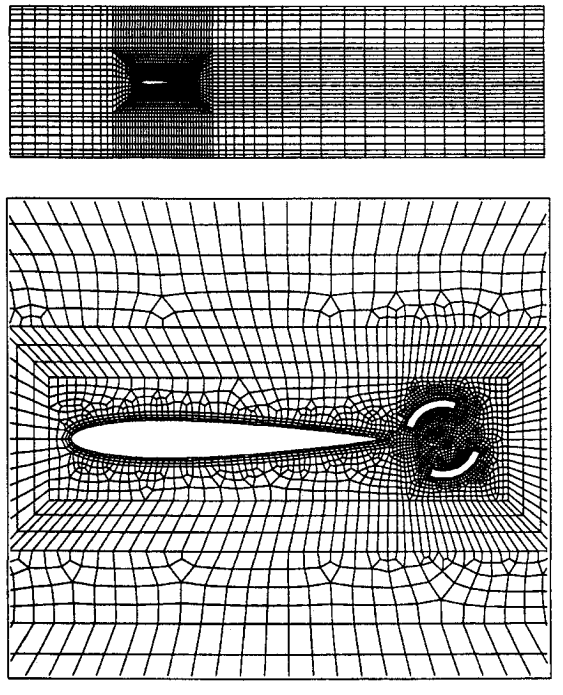

Fig. 2 Grid of the first configuration: a) entire domain and b) detail of airfoil and RSC.

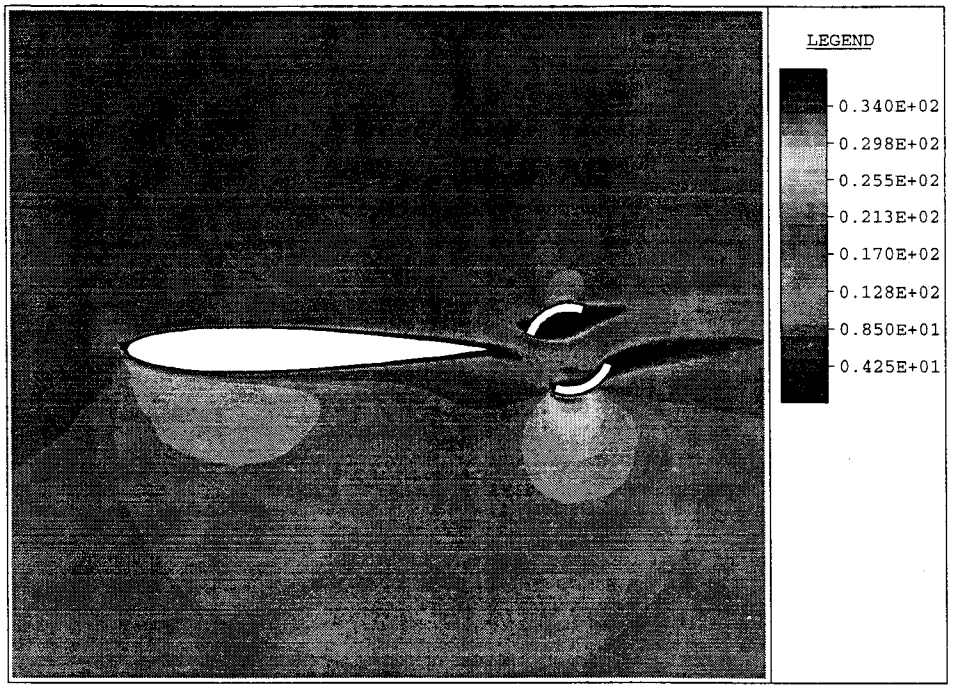

Fig. 3 Speed contour plot of the first configuration, u = 20 m/s, c = 102 mm, $\bar{d}$ = 0.25, $\bar{t}_C$ = 0.0245, θ = 70 deg, and $\bar{e}$ = 0.08.

accelerated on the lower side of the lower half of the RSC. The position of the RSC forces the flow to accelerate on the lower side of the airfoil, and as a result, the lift on the airfoil is pointed downward. In addition, the speed contour in the vicinity of the leading edge shows that the flow incidence is negative.

The lift variation of the airfoil/RSC system as a function of gap is presented in Fig. 4. One observes that the lift varies rapidly for small values of the gap, whereas for gap values larger than 20% of the chord, the lift is approximately constant. The same variation is observed for the airfoil lift. The lift on the RSC is almost constant as the gap value varies. The drag variation is presented in Fig. 4. As expected, the drag of the airfoil/RSC system is mainly because of the RSC. One observes that the drag of the RSC has the minimum for a small value of the gap (about 5% of the chord). For gap values larger than 7% the drag of the RSC is approximately constant. The airfoil drag is much smaller than the drag on the RSC. It is interesting to observe that for small values of the gap (under 5% of the chord) the airfoil diminishes the drag of the airfoil/RSC system.

Isolated RSC

In the second configuration, the variation of the RSC lift and drag is calculated for different rotation angles, from 0 to 180 deg. The angular difference between two successive positions is 10 deg. The distance between the inlet section and the RSC center is constant and equal to 547 mm.

The boundary and initial conditions are the same as for the first configuration. Several grid discretizations were tested, as presented in Fig. 5. As in the case of the first configuration, the chosen mesh is a combination of paved and mapped grid. The paved grid with three boundary-edge layers is used around the RSC while the mapped grid discretizes the rest of the domain.

The variations of lift and drag coefficients, using the RSC diameter as reference length, are presented in Fig. 6. As mentioned in the section about the model, because of the RSC symmetry, only the configurations corresponding to 0–180-deg rotation angle must be computed. More than that, because of the symmetry of the boundary and flow conditions, the lift and drag computation can be limited to 0–45 and 90–135 deg only.

The results presented in Fig. 6 were computed for the 0–180-deg domain. As anticipated, the lift and drag variation can be divided into two domains. The first domain spans from 0 to 90 deg, and the second spans from 90 to 180 deg. The lift is antisymmetric in both domains, the points of antisymmetry being 45 and 135 deg. The drag is symmetric in both domains, the points of symmetry being the same as the points of antisymmetry for the lift.

The lift variation is about the same in the first and the second domains. The maximum rate of the lift variation is much higher in the first domain than the maximum rate in the second domain. The drag variation is larger in the first domain. The minimum drag value corresponds in both domains to the zero-lift configuration. Also, the minimum drag value corresponds to the symmetry points, reinforcing the principle that symmetric flow configurations minimize the dissipated energy.

Effect of RSC Rotation Angle

In the third configuration, the variation of the lift and drag with the rotation angle was examined for a fixed value of the gap between the airfoil and the RSC. The position of the RSC varies from 0 to 180 deg. The angular difference between two successive positions is 10 deg. The gap between the airfoil and the RSC is constant and equal to 8.3 mm (about 8% of the airfoil chord).

The boundary and initial conditions are the same as for the previous two configurations. Similar to the previous two cases, the mesh is a combination of paved and mapped grids, as shown in Fig. 2.

As in the case presented previously of the RSC alone, the variation of the lift and drag for the airfoil/RSC configuration can be divided into two domains. The first domain spans from 0 to 90 deg, and the second domain spans from 90 to 180 deg. In the first domain the drag is symmetric and the lift is antisymmetric with respect to the position of 45 deg. In the second domain the point of symmetry for the lift and antisymmetry for the drag corresponds to a rotation angle of 135 deg.

It is interesting to observe from Fig. 7 that the absolute value of the lift on the RSC decreases by about 10% compared to the lift on the isolated RSC (second configuration). However, because of the airfoil, the total lift on the airfoil/RSC configuration is more than double the lift on the isolated RSC. The variation of the drag with the rotating angle is also shown in

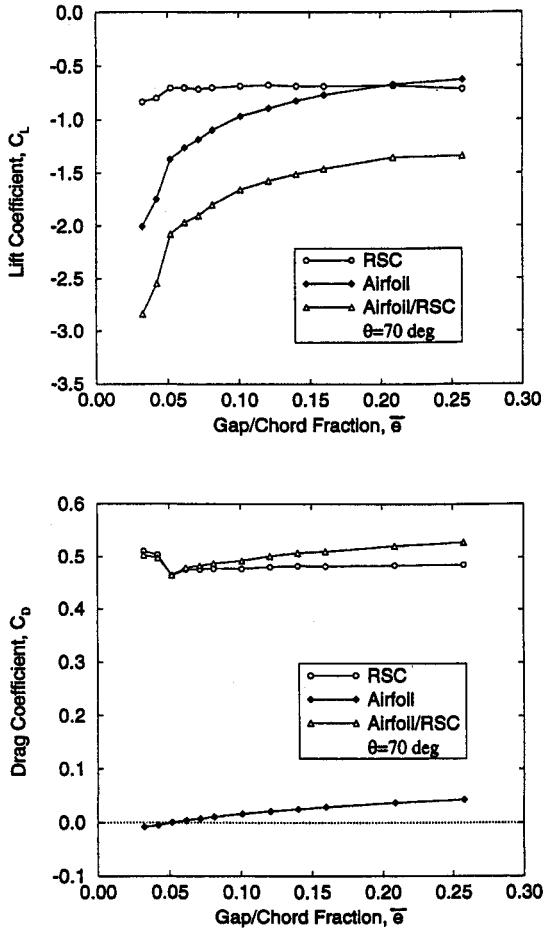

Fig. 4 Variation of lift and drag coefficients as a function of gap for the first configuration, u = 20 m/s, c = 102 mm, $\bar{d}$ = 0.25, t_c = 0.0245, and θ = 70 deg.

Fig. 7. The drag of the airfoil/RSC is smaller than the drag of the isolated RSC, with the drag reduction varying from 20 to 35%, depending on the rotation angle. One can conclude that the airfoil installed in front of the RSC has a positive effect on the lift as well as on the drag of the airfoil/RSC configuration. For this configuration, the drag force variation is about one-third of the lift force. This results in a fore and aft force at twice the frequency of the lift force. This force variation may be problematic for the gust generator system.

Grid Refinement Study

To validate the numerical results, grid refinement studies were done. For brevity, this report presents only the grid refinement study for the second configuration, the isolated RSC. Because the number of elements is large even for the so-called coarse grid (2942 elements and 2905 nodes), only the mesh around the RSC was varied while the rest of the grid was kept constant. The medium grid has 3977 elements and 3920 nodes. The fine grid has 5495 elements and 5414 nodes. Details of the grid for the coarse and fine grids are presented in Fig. 5.

The lift and drag values, presented in Fig. 8, show a very good agreement among the three grids. However, there is an important difference in computing time and memory between the three meshes, as can be seen in Table 1. This suggests that the coarse grid, which gives results that are very similar to those from the medium and the fine grids, should be used for computing the lift and drag variation as a function of the rotating angle. The computing time values presented in Table 1 were obtained using a Silicon Graphics Indigo 4400 computer.

The numerical results were also compared with the experimental data. The reader is referred to a companion paper[2] for the detailed comparison. For the purpose of illustrating this

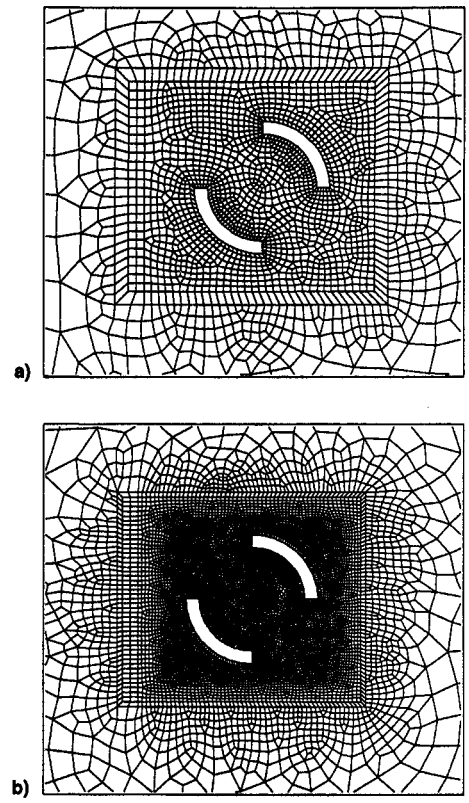

Fig. 5 Details of the grids used to test the grid convergence for the second configuration, isolated RSC: a) coarse and b) fine grids.

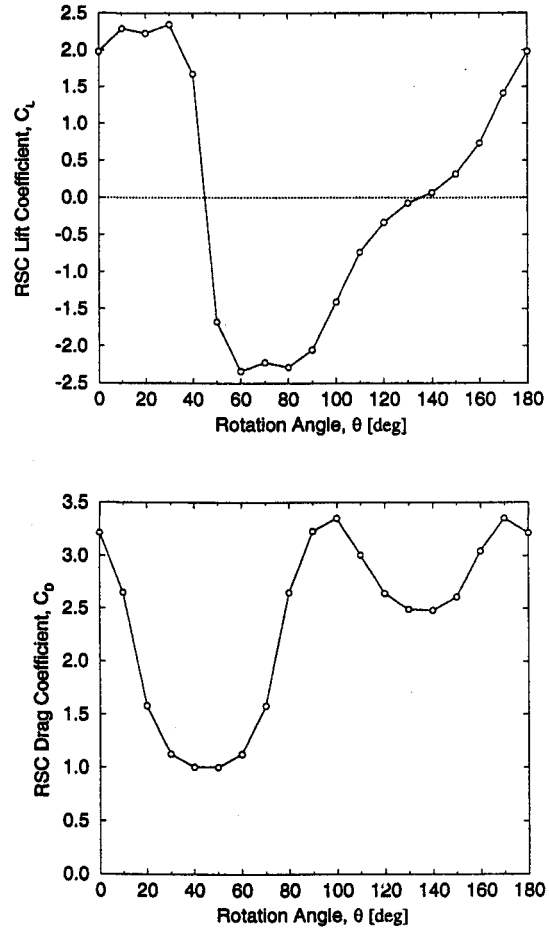

Fig. 6 Lift and drag coefficients of the isolated RSC vs θ.

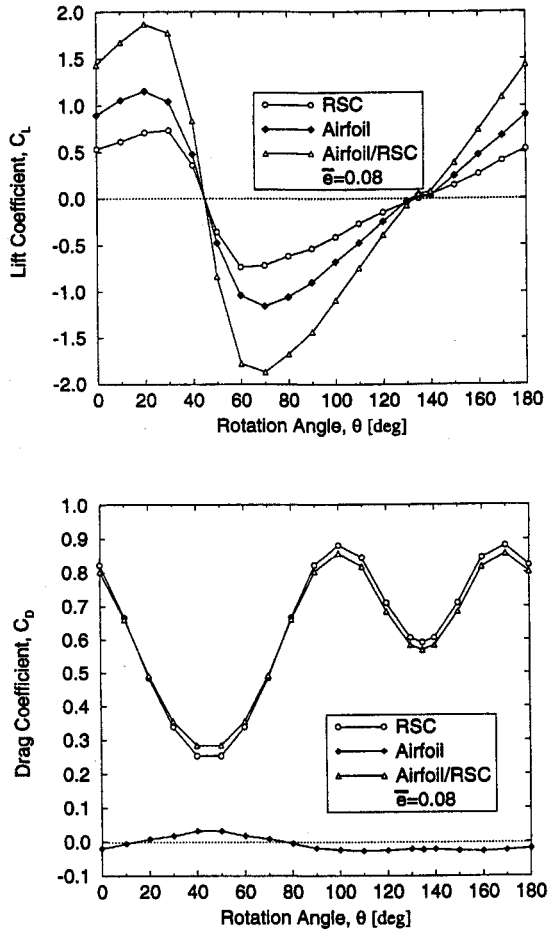

Fig. 7 Lift and drag coefficients of airfoil and RSC vs RSC θ, u = 20 m/s, c = 102 mm, $\bar{d}$ = 0.25, $\bar{t}_C$ = 0.0245, and $\bar{e}$ = 0.08.

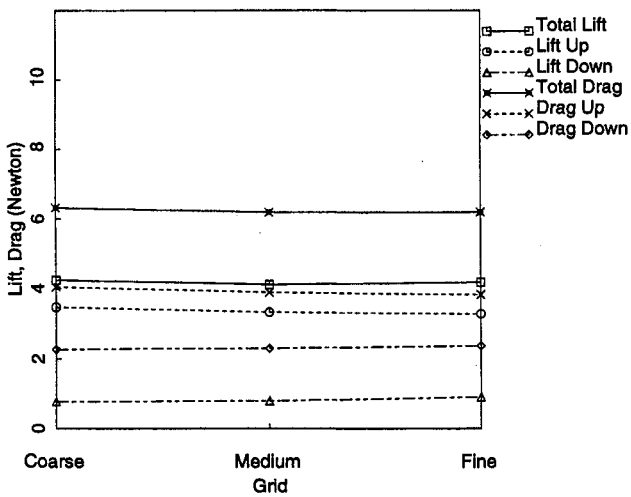

Fig. 8 Lift and drag for three grids of the second configuration.

comparison here, Fig. 9 shows the numerical and experimental lift variation of a slotted cylinder–airfoil combination as a function of the RSC rotation angle. In this case, the chord of the airfoil is c = 304.8 mm, the exterior diameter of the RSC is d = 76.2 mm, and the interior diameter is 57.1 mm. The gap between the airfoil trailing edge and the RSC is 24.4 mm. The numerical and experimental results are close, except in the vicinity of the rotation angle θ = 20 deg, where the pressure

Table 1 Variation of computing time in the grid refinement study

Grid	Nodes	Elements	Equations	Time/iteration, s
Coarse	2,905	2,942	10,452	91
Medium	3,920	3,977	14,312	203
Fine	5,414	5,495	20,048	555

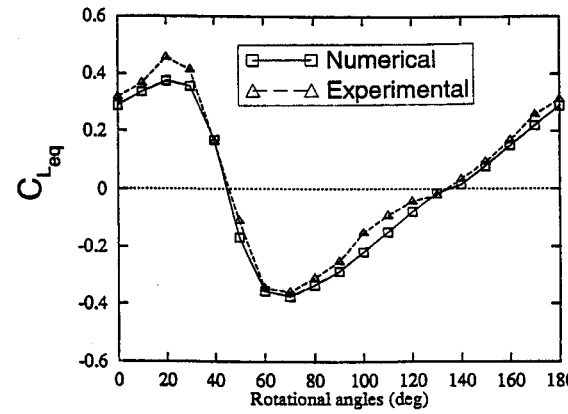

Fig. 9 Experimental and numerical equivalent lift coefficients of slotted cylinder–airfoil combination vs RSC θ, u = 20 m/s, c = 305 mm, $\bar{d}$ = 0.25, $\bar{e}$ = 0.08, and $\bar{t}_C$ = 0.0313.

distribution on the airfoil surface is particularly sensitive to the RSC position.

Concluding Remarks

The flow around an airfoil/RSC system was computed assuming that the flow is quasisteady, turbulent, and two dimensional. The lift and drag were calculated as a function of the rotation angle and as a function of the gap between the airfoil and the RSC. As expected, the lift and drag variation were periodic in the rotation angle and two different patterns repeated after each 180 deg of rotation angle.

To validate the computational results, wind-tunnel experiments for the airfoil/RSC were performed. The experiments provide not only the lift and the drag variation, but also the real boundary conditions for the turbulent kinetic energy and its dissipation rate at inlet. The comparison of the theoretical and experimental results[2] generally validates the numerical results. The numerical simulation can now be used to investigate other possible configurations for the RSC.

References

[1]Reed, W. H., III, "Flutter Exciter," U.S. Patent 4,809,553, March 7, 1989.

[2]Tang, D. M., Cizmaş, P. G. A., and Dowell, E. H., "Experiments and Analysis for a Gust Generator in a Wind Tunnel," *Journal of Aircraft*, Vol. 33, No. 1, 1996, pp. 139–148.

[3]Launder, B. E., and Spalding, D. B., "Turbulence Models and Their Applications to the Prediction of Internal Flows," *Proceedings of Symposium on Internal Flows*, Univ. of Salford, Salford, England, UK, 1971, pp. 1–15.

[4]Nallasamy, M., "A Critical Evaluation of Various Turbulence Models as Applied to Internal Fluid Flows," NASA TP 2474, May 1985.

[5]*FIDAP 7.0 Theory Manual*, Fluid Dynamics International, Evanston, IL, April 1993.

[6]Bercovier, M., and Engelman, M. S., "A Finite Element for Incompressible Fluid Flows," *Journal of Computational Physics*, Vol. 30, No. 2, 1979, pp. 181–201.

[7]Blacker, T. D., and Stephenson, M. B., "Paving: A New Approach to Automated Quadrilateral Mesh Generation," *International Journal for Numerical Methods in Engineering*, Vol. 32, No. 4, 1991, pp. 811–847.